



Microstructure, Corrosion and Electrochemical Properties of Cu/SiC Composites in 3.5 wt% NaCl Solution

M. M. Sadawy^{1,2} · Saad. M. Fayed¹ · Mahmoud Tayea² · I. G. El-Batanony²

Received: 8 May 2023 / Accepted: 7 August 2023 / Published online: 22 September 2023
© The Author(s) 2023

Abstract

This study investigated the role of SiC as a reinforcement on microstructure, corrosion, and electrochemical properties of Cu/xSiC ($x = 0, 5, 10, 15, 20, 25,$ and 30 vol% SiC) composites. The powder metallurgy route was used to fabricate Cu/SiC composite. The distribution of SiC reinforcing particles in the Cu matrix and their interfaces were investigated using optical and SEM/EDS microscopes. The various phases of Cu strengthened with SiC particles were detected using an X-ray diffractometer. The anticorrosion behavior and electrochemical properties of composites were investigated using various electrochemical techniques in 3.5 wt% NaCl solution. The electrochemical studies showed that the inclusion of SiC particles in the Cu matrix improved the resistance to corrosion. It was found that as the reinforcing particles increased to 20 vol%, the corrosion potential increased from -240 to -183 mV_{Ag/AgCl}, and the corrosion current density decreased from 5.01 to 0.02 $\mu\text{A cm}^{-2}$, while the passive current density decreased from 17.58 to 4.74×10^{-4} A cm^{-2} . This behavior resulted from the nucleation and production of a good protective layer. On another side, increasing reinforcing particles over 20 vol%, the corrosion current density increased from 0.05 to 0.63 $\mu\text{A cm}^{-2}$, while the corrosion potential shifted from -196 to -206 mV_{Ag/AgCl}.

Keywords Cu/SiC composite · SiC reinforcing particle · Relative density · Hardness · Corrosion · Pitting

1 Introduction

Copper is commonly employed in various applications due to its excellent thermal, electrical, and mechanical properties [1–5]. However, it has significant restrictions that limit the applications of pure copper, such as low yield strength, low hardness, and limited wear resistance ability. Reinforcing particles, such as alumina [6, 7], titanium carbide [8], tungsten carbide [9], and silicon carbide [10], can overcome these limitations and improve these properties. Material costs, production techniques, and applications should be considered when choosing the reinforcement elements which act as a carrying load into the composite [11]. Due to

their special characteristics like high hardness and strength, outstanding resistance to oxidation and corrosion, low coefficient of thermal expansion, and excellent heating transfer capacities, silicon carbide particles are a viable reinforcement for Cu-matrix among the other reinforcements [12–14].

Conventionally, metal matrix composites (MMCs) are widely prepared using casting or powder metallurgy techniques. The casting technique is a proper method for enhancing the mechanical and chemical properties [15, 16]. However, difficulties in controlling the mixing constituents and the distribution of reinforcement particles reduce its application in copper matrix composites [17]. Powder metallurgy is one of the most widely used techniques for producing composites reinforced with dispersion particles to a relatively soft metal matrix such as copper [11, 14, 18]. The inclusion of reinforcing particles with copper improves the composite properties [6–10]. Most MMCs have numerous advantages, such as good corrosion resistance, excellent wear, extremely good creep resistance, high-temperature operating ability, and superior dimensional stability [19]. It was reported that incorporating SiC into the copper matrix as reinforcement particles reduced the relative density and

✉ M. M. Sadawy
mosaadsadawy@yahoo.com

✉ Saad. M. Fayed
eng.saadfayed89@yahoo.com

¹ Mining and Petroleum Department, Faculty of Engineering, Al-Azhar University, Nasr City, Cairo 11371, Egypt

² Mechanical Department, Faculty of Engineering, Al-Azhar University, Nasr City, Cairo 11371, Egypt

electrical conductivity while the hardness was improved [5]. Further, Akbarpour et al. [20] illustrated that SiC improved the density, hardness, and abrasive wear resistance of the Cu-matrix. In addition, Metwally et al. [11] showed that the abrasive wear resistance of the Cu -matrix increased as the SiC increased in the composites due to grain refining of the matrix and the pinning effect of SiC.

On the other hand, corrosion can be considered a main factor for evaluating the application of composites as structural materials in marine environments [21]. Many parameters, such as volume fraction, reinforcement distribution, microstructure, and production method, can control the corrosion rate of composites. Further, some investigators found that pitting is the most common corrosion form in different composites [22, 23]. Torabi and Arghavanian [24] investigated the effect of SiC on the corrosion properties of Cu-10Sn alloy. Their results revealed that incorporating SiC particles to 10 wt% as a reinforcement increased the corrosion resistance and accelerated the protective film nucleation; above this value, the SiC particles reduced the corrosion resistance owing to particle agglomeration and incomplete composite sintering.

In fact, there are several studies on low-volume fractions of micro or/nano size SiC which deal with microstructure, mechanical, and physical/chemical properties of copper composite fabricated using powder metallurgy technique [25, 26]. However, few papers have been published on the corrosion behavior of copper reinforced with high-volume fractions of SiC particles. Unfortunately, low studies are offered which could attribute the influence of different proportionate additions from SiC particles to the Cu-base matrix on its corrosion behavior. Therefore, this study aims to examine the role of these particles in the range of (0–30 vol% SiC) on the microstructure, corrosion, and electrochemical properties of Cu/SiC composites in 3.5 wt% NaCl solution.

2 Material and Procedure

2.1 Materials

Cu powder (4 μm) strengthened with SiC particles (2.5 μm) were produced by the powder metallurgy method. Reinforcing particles were utilized in volume percentages (%) ranging from 0 to 30%. Figures 1 and 2 show the properties of the powders utilized in the investigation. The powder was carefully weighed to the requisite % utilizing an electronic balance with a precision of ± 0.01 mg. The powders were blended for 3 h in a closed mixer to obtain a homogeneous distribution of

the reinforcing particles within the MMCs. The powders were cold compressed on a disc steel die with a diameter of 12 mm and a thickness of 10 mm using a universal testing machine at an axial pressure of 450 MP. The compressed specimens were sintered for 2 h in an electric tube furnace at 850 ± 5 °C with argon gas with a flowing rate of 1 L/min.

2.2 Characterization

The pure Cu and Cu/SiC composite microstructures were investigated using the optical microscope model (Zeiss) and scanning electron microscope (SEM) model (JEOL JSM-6330F). According to ASTM E3-95 [27], all specimens were ground with sandpaper of SiC ranging from 180 to 2000#. After that, the specimens were cloth polished using 1 μm diamond paste. The specimens were cleaned in an acetone solution and air-dried. Energy dispersive spectroscopy (EDS) was carried out to identify the content of Cu, SiC, and Cu/SiC sintered composite.

2.3 XRD

The multi-phases of Cu matrix strengthened with SiC particulates were measured using an X-ray diffractometer (XRD, Philips Analytical X-ray B.V. Machine). The detection range was from 10 to 90° of (2 θ) with a step size of 0.05° (2 θ) and a measuring time of 5 s/step.

2.4 Relative Density and Porosity

The relative densities (ρ_{rel}) of the pure Cu and Cu/SiC composites were estimated by utilizing the following Eq. (1):

$$\text{Relative density} = \frac{\rho_{\text{exp}}}{\rho_{\text{th}}} \times 100 \quad (1)$$

where ρ_{exp} is the measured or experimental density and ρ_{th} is the theoretical density of the specimens. The experimental density of the sintered specimens was determined using the Archimedes method. The theoretical density was determined using Eq. (2) [28]:

$$\text{Theoretical density} = \frac{100}{\left[\frac{W_{\text{Cu}}}{\rho_{\text{Cu}}} + \frac{W_{\text{SiC}}}{\rho_{\text{SiC}}} \right]} \quad (2)$$

where ρ is the density, and W denotes the weight fractions, respectively. The porosities of the sintered specimens were estimated by utilizing the rule of the mixture as indicated in the next Eq. (3):

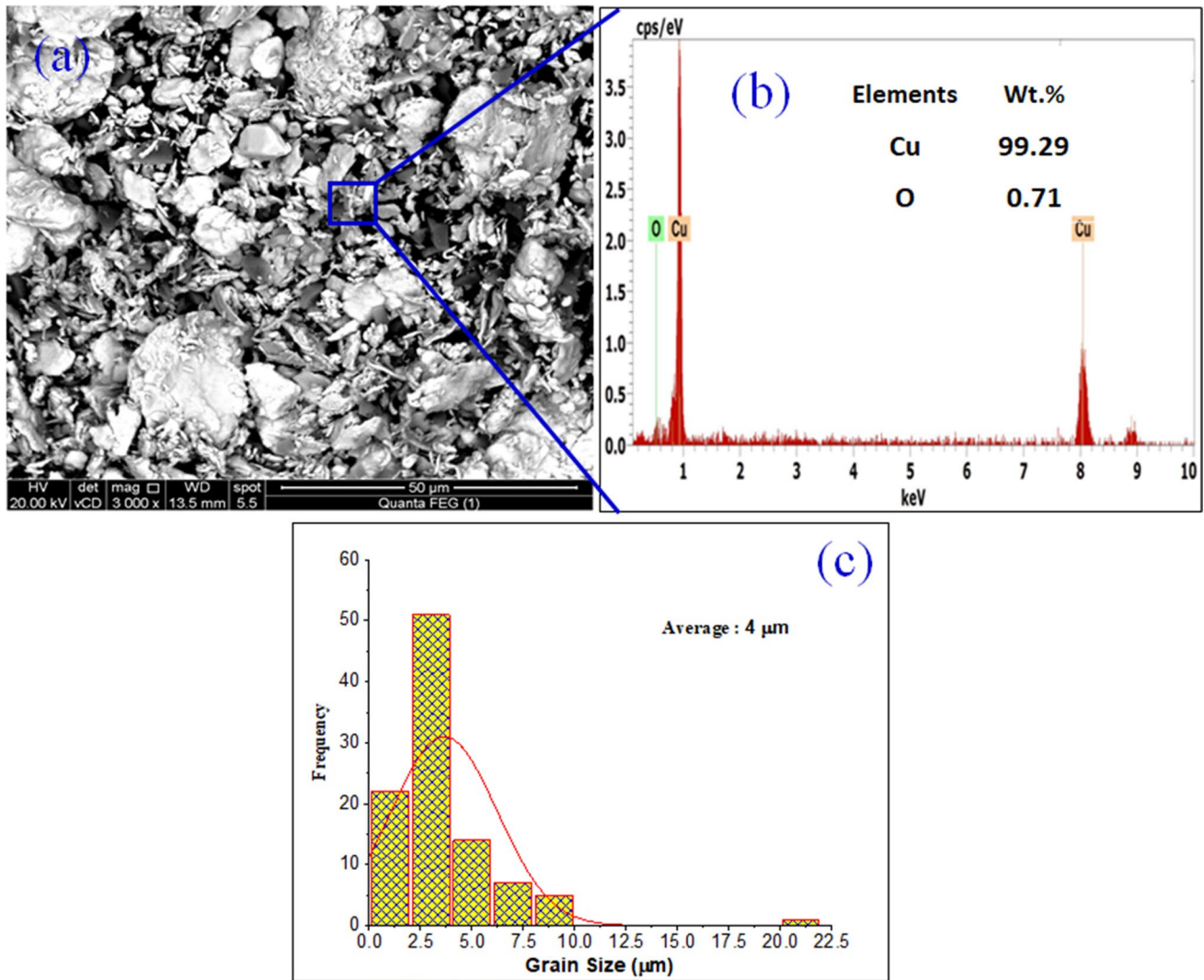


Fig. 1 The SEM image, EDS analysis and particle size distributions of the SiC powder

$$\text{Porosity} = \left[1 - \frac{\rho_m}{\rho_t} \right] \times 100 \quad (3)$$

where ρ_m signifies the density as measured, and ρ_t represents the density as theoretically.

2.5 Hardness

The Vickers indentation technique was used to determine the hardness of specimens with a load of 5 kg for Cu/SiC composites. The exact hardness of each specimen was determined by averaging ten measurements for each specimen.

2.6 Immersion Corrosion Tests

According to ASTM G1 and G31 [29, 30], the specimens were soaked in a solution containing 3.5 wt% NaCl at 25 °C

to obtain the corrosion rate. The specimens were ground with SiC sandpaper to 1200# to get a mirror surface. All specimens were ultrasonically cleaned in an acetone bath, de-ionized water, and then air-dried. Before immersion in the solution, the beginning weights of the specimens (W_0) were measured with an analytical balance (accuracy: ± 0.001 mg). The specimens were immersed in the chloride solution for an interval time of (72–576) h. After the expiration of the time, the specimens were removed from the solution. The corroded specimens were submerged in concentrated HNO_3 for 3 min to remove the corrosion products. The difference in weight (final and initial weight) was used to calculate the mass loss for each specimen. The corrosion rate was calculated using Eq. (4) [29]:

$$r = \frac{K \times \Delta W}{A \times D \times t} \quad (4)$$

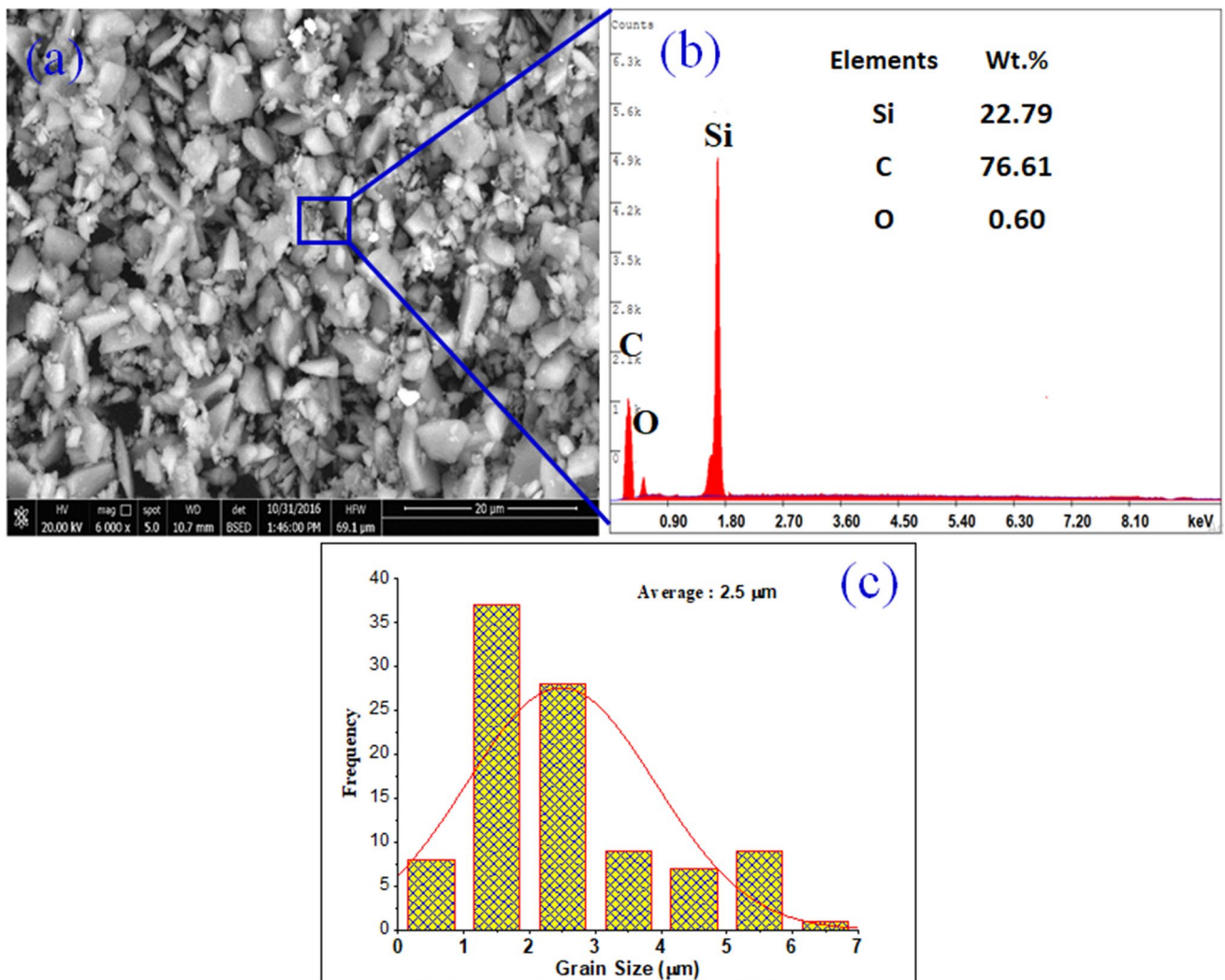


Fig. 2 The SEM image, EDS analysis and particle size distributions of the Cu powder

where K is a constant (8.76×10^4), ΔW is the weight loss (mg), r is the corrosion rate ($\text{mm} \cdot \text{y}^{-1}$), A is the area (cm^2), D is the density of the specimen (g/cm^3), and t is the exposure time (h).

2.7 Electrochemical Measurements

Potentiostat/Galvanostat (EG&G model 273) was used to perform potentiodynamic polarization, cyclic polarization, and potentiostatic tests, while Gamry Potentiostat/Galvanostat (PCI300/4) was used for electrochemical impedance

Table 1 Relative density, and porosity Cu composite reinforced with different SiC content

Serial no	Composites	Theoretical density (g/cm^3)	Measured density (g/cm^3)	Relative density (%)	Porosity (%)
1	Cu/0SiC	8.96	8.48 ± 0.01	94.64	5.36 ± 0.01
2	Cu/5SiC	8.66	8.07 ± 0.03	93.18	6.82 ± 0.04
3	Cu/10SiC	8.36	7.65 ± 0.02	91.507	8.49 ± 0.03
4	Cu/15SiC	8.08	7.38 ± 0.06	91.336	8.66 ± 0.05
5	Cu/20SiC	7.80	7.02 ± 0.07	90.00	10.00 ± 0.03
6	Cu/25SiC	7.55	6.62 ± 0.08	87.68	12.32 ± 0.09
7	Cu/30SiC	7.23	6.25 ± 0.09	86.44	13.56 ± 0.1

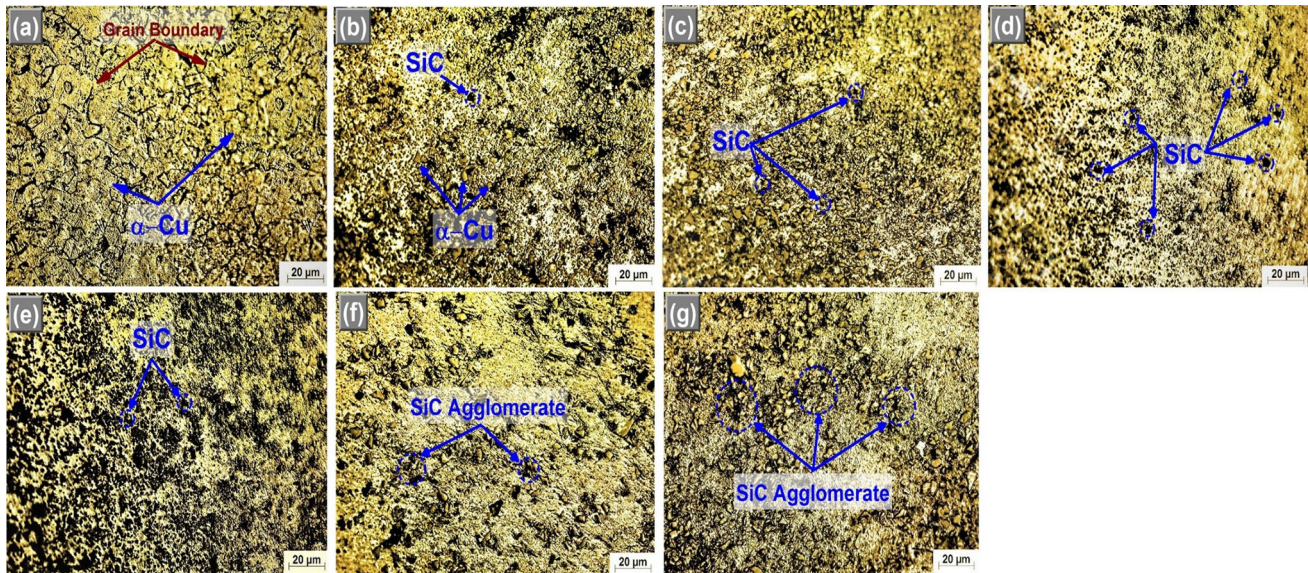


Fig. 3 Optical micrographs of Cu composites reinforced with various SiC content (a 0 vol%, b 5 vol%, c 10 vol%, d 15 vol%, e 20 vol%, f 25 vol%, and g 30 vol% of SiC particulates)

spectroscopy (EIS) measurements The electrochemical cell composed of three-electrodes: Cu/SiC specimens with an exposed surface area of 1.0 cm^2 as the working electrode, Pt sheet with a surface area of 2 cm^2 as a counter electrode, and Ag/AgCl as the reference electrode. The electrochemical trials were conducted in a corrosive environment (3.5 wt% NaCl solution). The EIS measurements were taken at the 30 min open circuit potential. The applied voltage was 10 mV in amplitude and ranged from 0.01 Hz to 100 kHz in frequency. The Echem Analyst software was used to evaluate the impedance data. Potentiodynamic polarization experiments were performed at 0.5 mVs^{-1} scan rate. Although a 0.5 mVs^{-1} is adopted in this stage of the experimentations, it is remarked that potential scan rate has no substantial provided distortions in the polarization curves obtained, as previously reported [31–34]. Besides, no deleterious effect is verified when polarization parameters are obtained (e.g. corrosion current densities and potentials). However, it is worth noted that potential scan rate has an important role in order to minimize the effects of distortion in Tafel slopes and corrosion current density analyses, as previously reported [31–34]. The PAR Calc Tafel Analysis method was used to fits the corrosion results based on the Stern-Geary model. Cyclic potentiodynamic plots were performed from $1.0 \text{ V}_{\text{Ag/AgCl}}$ across the anodic direction at a scanning rate of 0.25 mVs^{-1} . The scanning potential was reversed when the current density attained 10 mA cm^{-2} . After cyclic polarization measurements, the surface morphology and multiphases of corroded specimens were evaluated using a scanning electron microscope analysis and XRD. Potentiostatic tests were performed at $300 \text{ mV}_{\text{Ag/AgCl}}$ for 0.5 h. All tests

were done in triplicate for each experiment to ensure the validity of the results. The standard deviation value in each condition was calculated to assess the measurement error.

3 Results and Discussions

3.1 Microstructure Characterization

The effect of micro-sized SiC vol% on the relative density and porosity of Cu/SiC composites is illustrated in Table 1. It is clear that increasing SiC particles, declines Cu/SiC composites density. The relative density reduced from 94.64 (pure Cu) to 86.44% with increasing SiC particles to 30 (vol%). The high reduction in the relative density is attributed to the size and content of SiC, according to the conclusion of Efe et al. [35]. Further, the density of SiC particles (3.2 g/cm^3) is substantially less than that of Cu (8.9 g/cm^3), which explains this reduction in the density. The outcome is similar to the results of Prosviryakov [36]. On the other hand, the results show that the porosity of composites increases with increasing content of SiC particles. The behavior is attributed to Cu/SiC interface is high in composites with a high SiC content, resulting in a high copper atom diffusion barrier. The copper atoms are thus unable to disperse and seal the gaps between the SiC particles easily. Therefore, the densification is hindered [37, 38].

The optical micrographs of copper reinforced with various proportions of SiC particles are shown in Fig. 3. In general, the grains of the alloys are approximately equiaxed grain structures. The SiC particles are distributed within

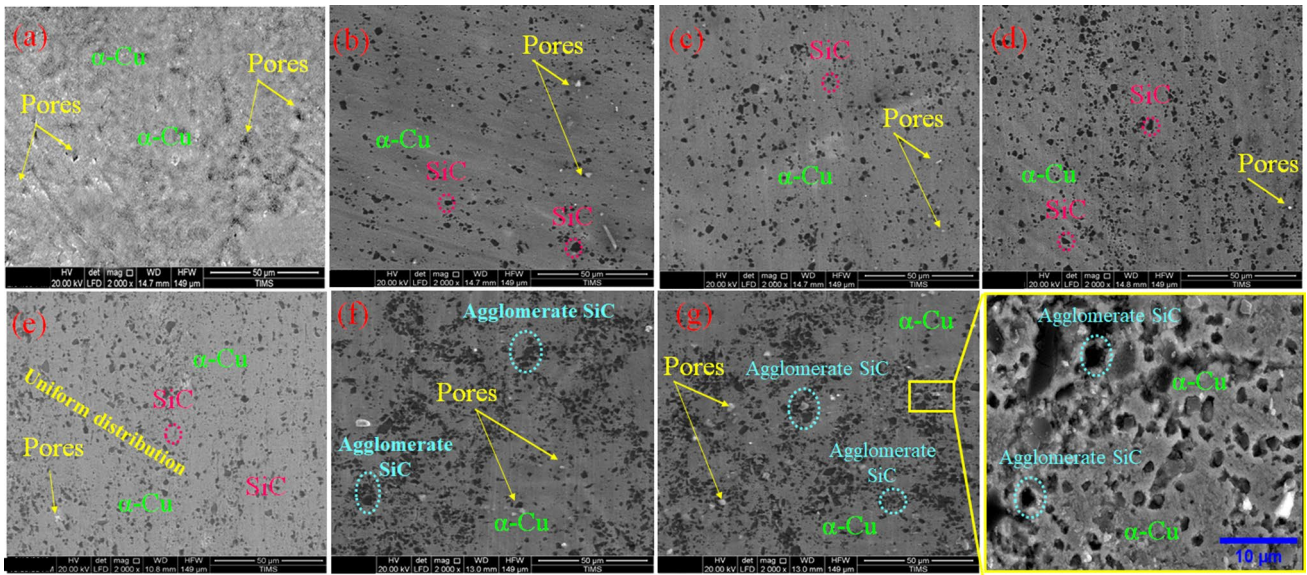


Fig. 4 SEM micrographs showing the dispersion of SiC microparticles in Cu matrix (a 0 vol%, b 5 vol%, c 10 vol%, d 15 vol%, e 20 vol%, f 25 vol%, and g 30 vol% of SiC particulates)

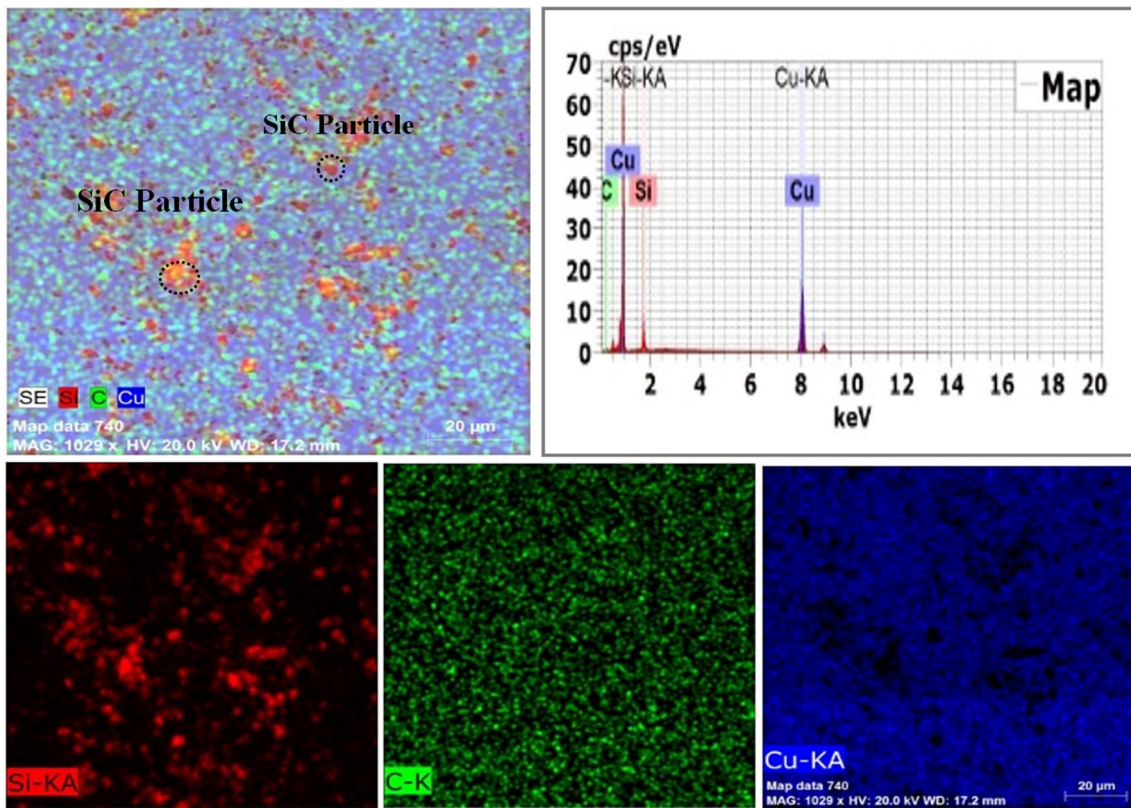
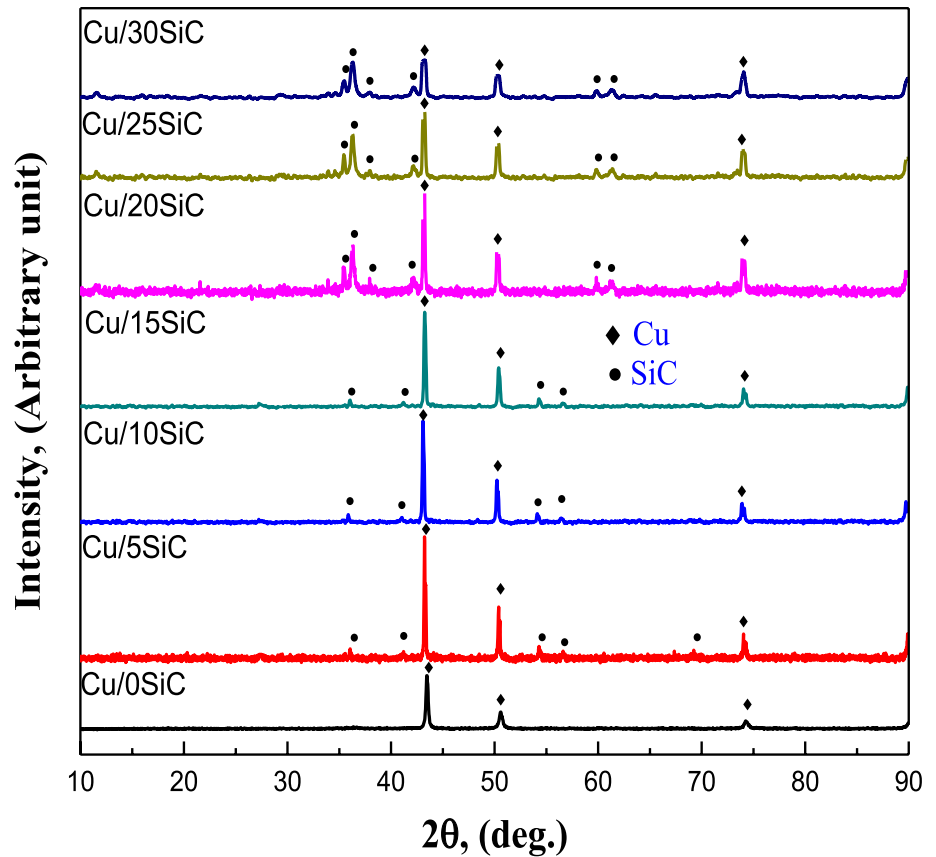


Fig. 5 EDS elemental mapping of Cu/20SiC micro-composites and their corresponding elemental mapping of Si, C and Cu respectively

the matrix. However, these images reveal some porosity. As shown in Fig. 3, the dark phase represents SiC dispersion in the composite, whereas the bright phase represents the

Cu matrix. The SiC volume fraction affects the morphology of MMCs grains. Figure 4 show the SEM images of the composites sintered at 860 °C for 2 h. The micrograph

Fig. 6 XRD patterns of Cu matrix strengthened with different vol% SiC particles



indicated that the pure copper specimen possessed a uniform homogeneous structure and included a single phase (Fig. 4a). Moreover, the porosity can be seen in a few places due to inadequate compacting, which admits air enters into the specimen. This air was trapped and released during the sintering process, creating porosity. Figure 4b–g shows Cu composites reinforced with various vol% of silicon carbide particles. The SEM micrographs of reinforced specimens showed that the metal matrix composite contains Cu and SiC particles. Moreover, the metal matrix exhibits improper dispersion of the reinforcing particle, most likely due to localized agglomeration. The SEM pictures of the Cu/5SiC composite specimen (Fig. 4b) demonstrated the presence of

copper in the bright area. In contrast, the dark area reflects the cluster of micro-SiC in a few sites. The absence of an intermediate phase in SEM images between the Cu and SiC interface suggests no reaction happened during the sintering process. The inclusion of SiC reinforcing particulates into the Cu matrix promotes grain refinement. Also, the microscopic image showed that when the SiC particle concentration increased, the distribution of particles became uniform up to 20 vol%. Additionally, the SEM image revealed that non uniform distributions could be observed above this value due to SiC agglomeration. Similar results were reported by Efe et al. [35, 39]. Figure 5 depicts the mapping EDS analysis of Cu/20SiC composites. The elements map reveals the

Table 2 Equivalent circuit parameters of Cu composite with different SiC contents

Samples	R_s ($\Omega \text{ cm}^2$)	R_{ct} ($\Omega \text{ cm}^2$)	Q_{dl}		W_d ($\text{Ss}^{1/2} \text{ cm}^{-2}$)	χ^2
			Y_0 (F cm^{-2})	n_1		
Cu/0SiC	12.2 ± 0.01	190 ± 6	220 ± 6	0.70 ± 0.01	0.04 ± 0.003	22×10^{-4}
Cu/5SiC	10.1 ± 0.02	230 ± 5	180 ± 4	0.76 ± 0.02	0.03 ± 0.002	19×10^{-4}
Cu/10SiC	9.1 ± 0.06	250 ± 10	160 ± 3	0.75 ± 0.04	0.02 ± 0.001	18×10^{-4}
Cu/15SiC	9.2 ± 0.04	260 ± 3	130 ± 2	0.8 ± 0.03	0.006 ± 0.0002	15×10^{-4}
Cu/20SiC	8 ± 0.01	422 ± 11	110 ± 2	0.88 ± 0.04	0.008 ± 0.0004	10×10^{-4}
Cu/25SiC	9.4 ± 0.02	350 ± 9	120 ± 3	0.82 ± 0.02	0.009 ± 0.01	13×10^{-4}
Cu/30SiC	10 ± 0.07	295 ± 8	125 ± 4	0.86 ± 0.01	0.07 ± 0.0001	14×10^{-4}

Fig. 7 Effect of SiC vol% on the Crystallite size and Lattice Strain

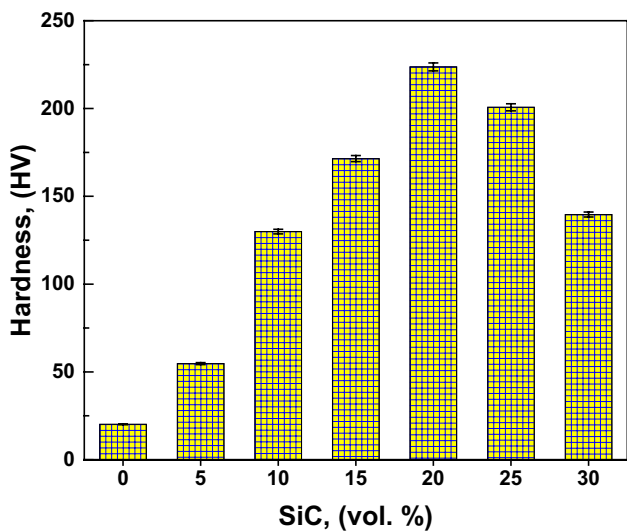
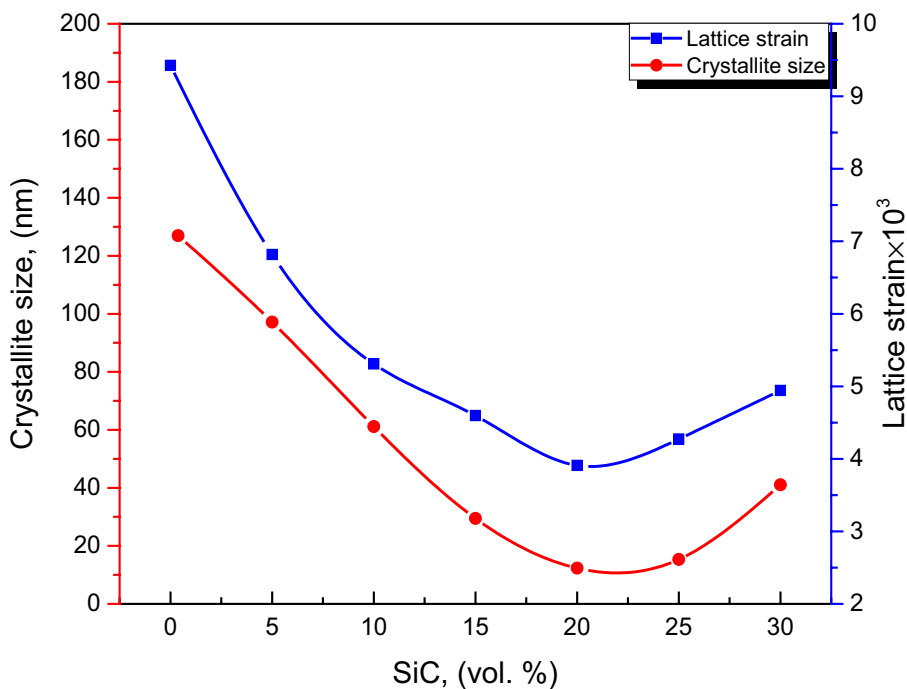


Fig. 8 Hardness of Cu matrix as a function of SiC vol% microparticles addition

presence of the Cu, Si, and C components in an SEM micrograph of the composite. Furthermore, the EDS analysis map demonstrates a uniform dispersion of SiC within Cu/20SiC micro composite [25].

Figure 6 shows the XRD spectrums of a Cu/SiC micro/composite with several of vol% of SiC particles. According to the Joint Committee of Powder Diffraction Standards (JCPDS) database, the reflection planes of (111), (200), and (220) at 2θ of 43.29, 50.43, and 74.12,

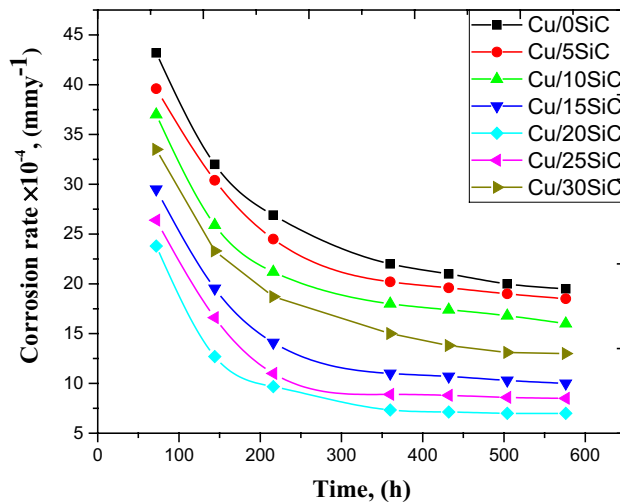


Fig. 9 Corrosion rate-time curves of Cu matrix reinforced with different SiC contents in 3.5 wt% NaCl solution

respectively, confirm the formation of Cu face center cubic. The reflection planes of (100), (002), (101), (102), and (110) at 2θ of 33.58, 35.50, 38.13, 49.67, and 60.05, respectively, confirm the formation of hexagonal SiC particles. Besides, XRD analysis confirmed that including more SiC particles in composites decreased the intensity of the Cu peaks. According to Akbarpour et al. [20], the decrease in intensity is caused by a difference in thermal expansion between the Cu matrix and the SiC particles, resulting in the creation of lattice micro-strain in the

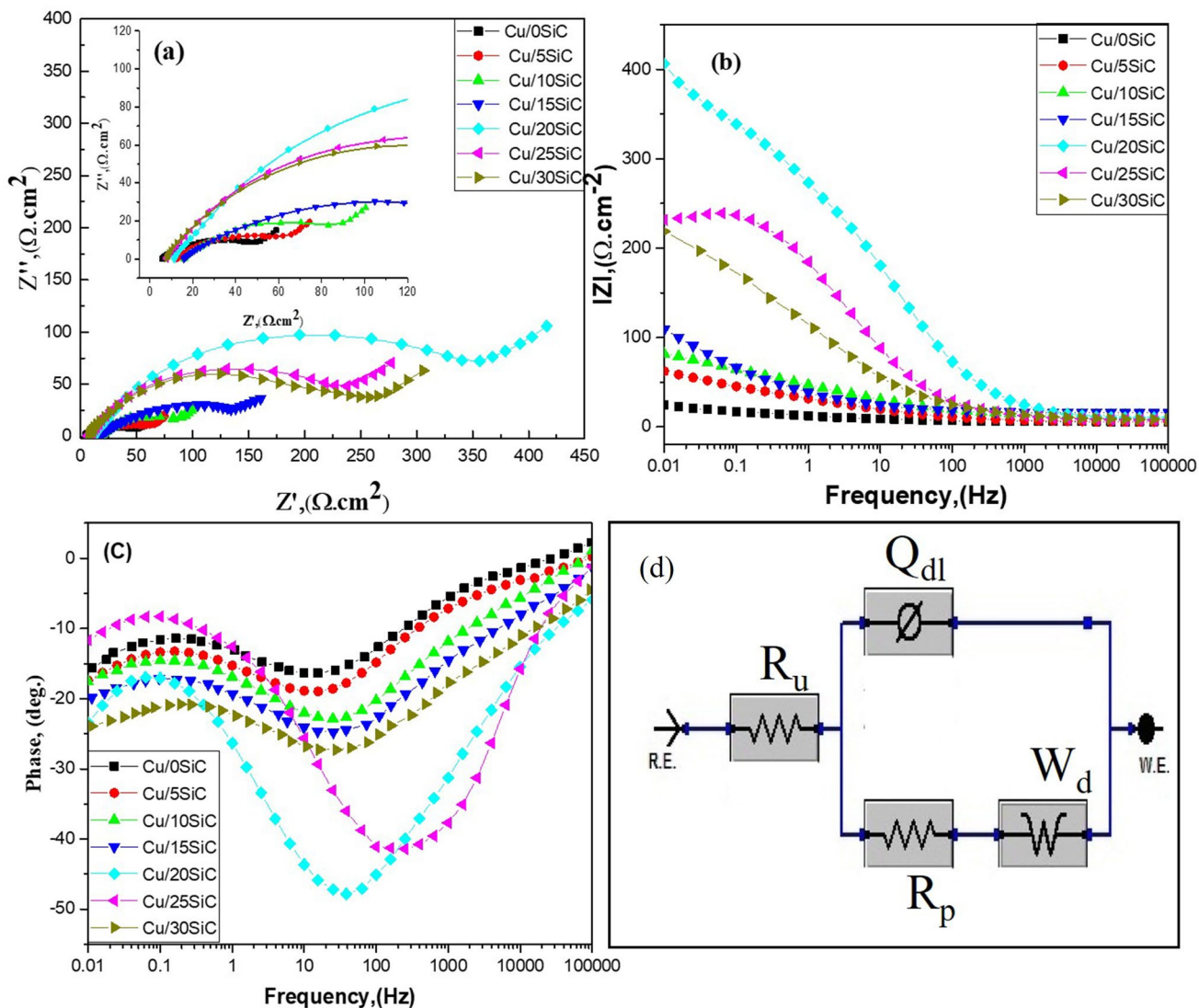


Fig. 10 Nyquist, and bode plots of Cu matrix with different SiC contents in 3.5 wt% NaCl solution. (a) Nyquist plot, b, c bode plot, d Electrical equivalent circuit

composite. In others words, the decreasing grain size of the matrix can also explain this behavior [40].

Moreover, the size of the crystallite (d) and lattice strain (η) of (α -Cu) matrix were determined by the Williamson-Hall formula Eq. (5):

Table 3 Potentiodynamic parameters of Cu composite reinforcement with different SiC contents

Samples	E_{corr} (mV)	i_{corr} ($A\ cm^{-2}$)	R_p (Ohm)	Corrosion rate ($mm\ y^{-1}$)	β_c (mV/decade)	β_a (mV/decade)
Cu/0SiC	-240 ± 8	$(5.01 \pm 0.05) \times 10^{-6}$	$(5.39 \pm 0.01) \times 10^3$	$(6.1 \pm 0.2) \times 10^{-2}$	124 ± 5	125 ± 2
Cu/5SiC	-235 ± 7	$(4.69 \pm 0.03) \times 10^{-6}$	$(7.01 \pm 0.01) \times 10^3$	$(5.78 \pm 0.3) \times 10^{-2}$	225 ± 6	106 ± 3
Cu/10SiC	-225 ± 3	$(0.21 \pm 0.001) \times 10^{-6}$	$(1.24 \pm 0.001) \times 10^5$	$(2.77 \pm 0.1) \times 10^{-2}$	127 ± 3	95 ± 7
Cu/15SiC	-195 ± 4	$(0.13 \pm 0.002) \times 10^{-6}$	$(2.40 \pm 0.003) \times 10^5$	$(1.76 \pm 0.2) \times 10^{-3}$	188 ± 4	99 ± 4
Cu/20SiC	-183 ± 5	$(0.02 \pm 0.002) \times 10^{-6}$	$(1.23 \pm 0.002) \times 10^6$	$(3.72 \pm 0.2) \times 10^{-4}$	146 ± 7	108 ± 5
Cu/25SiC	-196 ± 6	$(0.05 \pm 0.003) \times 10^{-6}$	$(7.70 \pm 0.002) \times 10^5$	$(7.96 \pm 0.11) \times 10^{-4}$	157 ± 8	117 ± 6
Cu/30SiC	-206 ± 8	$(0.63 \pm 0.001) \times 10^{-6}$	$(7.44 \pm 0.04) \times 10^4$	$(10.51 \pm .09) \times 10^{-4}$	139 ± 2	165 ± 8

Table 4 Cyclic polarization parameter of Cu composite reinforced with SiC particle in 3.5 wt% NaCl solution

Samples	E_{pas} (mV)	i_{pas} ($A\ cm^{-2}$)	E_{pit} (mV)	i_{pit} ($A\ cm^{-2}$)	E_{prot} (mV)	i_{prot} ($A\ cm^{-2}$)
Cu/0SiC	54.24 ± 3	$(2.95 \pm 0.14) \times 10^{-4}$	812.1 ± 10	$(1.38 \pm 0.1) \times 10^{-3}$	-89.55 ± 2	$(2.45 \pm 0.01) \times 10^{-7}$
Cu/5SiC	47.7 ± 2	$(2.34 \pm 0.12) \times 10^{-4}$	860 ± 11	$(1.20 \pm 0.09) \times 10^{-3}$	-83 ± 3	$(4.78 \pm 0.03) \times 10^{-7}$
Cu/10SiC	17.65 ± 1	$(8.31 \pm 0.13) \times 10^{-5}$	907 ± 15	$(1.0 \pm 0.03) \times 10^{-3}$	-148 ± 4	$(1.81 \pm 0.02) \times 10^{-7}$
Cu/15SiC	78 ± 4	$(1.58 \pm 0.10) \times 10^{-4}$	1122 ± 9	$(1.04 \pm 0.01) \times 10^{-3}$	-89.5 ± 6	$(1.99 \pm 0.01) \times 10^{-7}$
Cu/20SiC	23.9 ± 2	$(7.07 \pm 0.2) \times 10^{-5}$	1283 ± 8	$(8.12 \pm 0.01) \times 10^{-4}$	-77.07 ± 3	$(9.33 \pm 0.03) \times 10^{-8}$
Cu/25SiC	12.05 ± 3	$(8.51 \pm 0.25) \times 10^{-5}$	1259 ± 13	$(1.04 \pm .02) \times 10^{-3}$	-95.5 ± 3	$(1.28 \pm 0.02) \times 10^{-7}$
Cu/30SiC	41.7 ± 5	$(1.41 \pm 0.09) \times 10^{-4}$	1176 ± 14	$(1.04 \pm 0.03) \times 10^{-3}$	-137 ± 5	$(2.13 \pm 0.06) \times 10^{-7}$

$$\beta \cos \theta = \frac{k\lambda}{d} + 4\eta \sin \theta \quad (5)$$

where k is the Scherrer constant ($(k=0.9-1.0)$), λ denotes to X-ray wavelength, η represents the average of lattice strain, β is the full width at half maximum peaks in radian, and θ refers to Bragg angle. Plotting $\beta \cos \theta$ versus $\sin \theta$ for (α -Cu) gives a straight line with a slope of (2η) and intercept of $(k\lambda/d)$. The data used in Eq. (5) were obtained from Fig. 6. The crystallite size (d) and the lattice strain (η) were plotted in Fig. 7. The outcomes showed that the crystallite size of an α -Cu matrix is decreased by $\sim 36, 62, 66,$ and 72% for 5%, 10%, 15 and 20%vol SiC, respectively, compared with the pure Cu sample. Further, increasing the SiC particle to 25 and 30%vol increased the average lattice strain and the crystallite size by $\sim 29, 38,$ and $11, 32,$ respectively. This behavior is ascribed to the non-uniform distribution of SiC inside the matrix [11].

3.2 Hardness Measurements

Figure 8 depicts the hardness of composites strengthened with different SiC vol%. According to the observations, the pure specimen has a hardness of about 20.16 ± 0.1 HV. Additionally, Fig. 8 demonstrated that increasing the vol% of SiC increased the hardness of the composites. The results showed that increment the micro-sized SiC concentration to 5, 10, 15, and 20 vol% increased the average hardness values by 28, 39, 65, and 77%, respectively. The findings indicate that the hardness of pure Cu in HV is lower than that of micro/composite specimens owing to the existence of the ceramic phase (SiC) in the composite specimens. This improvement in hardness is attributable to the homogeneous dispersion of reinforcing particles (SiC) and good adhesion to matrix composites. Moreover, the inclusion of micro/size (SiC) particles within the composite works as a load-supporting element in micro composites, contributing to improved hardness. The inclusion of SiC particles above 20 vol% causes a reduction of hardness due to the accumulation of the particles and inadequate sintering of the

specimen. These findings are consistent with earlier research reported by various authors [41, 42].

3.3 Immersion Tests

The corrosion rate of Cu matrix reinforced with various vol% SiC particles as a function in immersion time is presented in Fig. 9. The outcomes reveal that as the soaking time extended, the corrosion rate of the specimens decreased and reached stable values. This behavior is due to creating of a thin passive film on the top surface of reinforced Cu composite alloy. These films operated as a physical barrier, impeding charge transfer throughout the corrosion products and lowering the corrosion rate. Further, the outcomes showed that the corrosion rate of Cu/20SiC has a lower corrosion rate when compared to other specimens. Moreover, the results revealed that the Cu/20SiC specimen had the lowest corrosion rate compared to the other specimens. The enhancement in corrosion resistance is due to the high purity of SiC, its chemical stability, and the homogenous dispersion of reinforcing particles in the Cu composite. Because of this, the micro galvanic coupling between the reinforcing particles and the Cu matrix has been significantly reduced. Additionally, incorporating reinforcing particles (SiC) above 20% increases the composite corrosion rate owing to SiC clustering in copper matrix composites [43, 44].

3.4 Electrochemical Impedance Spectroscopy (EIS)

The technique of electrochemical impedance spectroscopy was employed to investigate corrosion characteristics at the Cu/SiC composite/electrolyte interface. The Nyquist and Bode plots of Cu/SiC composite alloys in 3.5 wt% NaCl aqueous solution are shown in Fig. 10a–c. The Nyquist graphs revealed that the specimens display a capacitive arc in the high-frequency and a straight line in the low-frequency. The capacitive arc in the high-frequency range is related to the resistance to charge transfers at metal/electrolyte contact. A greater capacitive arc diameter indicates

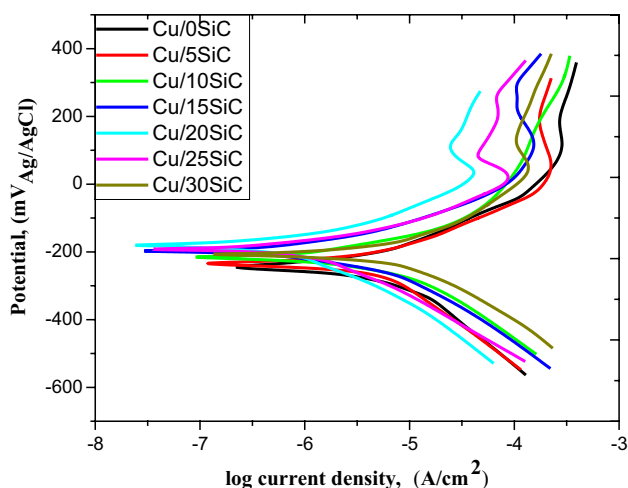


Fig. 11 Potentiodynamic polarization plots of Cu matrix strengthened with different vol% of SiC in 3.5 wt% NaCl solution

better corrosion resistance. This means that the impedance modulus of specimens increased with rising SiC content, up to 20%, as seen in Fig. 10a. The straight line indicates Warburg impedance, in which Cu composite diffuses anodically from the specimen into the bulk solution, whereas oxygen diffuses cathodically from the bulk solution onto the specimen. On another side, Fig. 10b, c illustrates the bode spectra for the Cu/SiC composite specimen in 3.5 wt% NaCl solution. The spectra shows single constant time in the whole frequencies. Further, it is apparent that the Cu/20SiC composite specimen has a larger phase angle at the mid-frequency than the other composite specimens. Thus, this behavior is ascribed to the creation of a passivating layer on the surface of the specimens and enhanced anticorrosion in the defect areas [45, 46]. On the other hand, when Nyquist plots at high frequency domain are analyzed, it is suggested that all examined specimens characterize a porous electrode behavior. This is based on the fact that at high frequency domain, straight lines forming 45° are characterized. This is mainly when 20, 25 and 30 SiC contents are considered. This indicates that the effect of porous electrode is higher than other examined specimens. However, these also demonstrate porous electrode behavior, which is characterized at 22.5° , as also previously reported [47]. Based on this, it is stated that the electrochemical behaviors of all examined specimens are prevalent with both planar and porous electrode. At low frequency domain, these examined specimens depict slopes at 45° , indicating a possible charge and transport/diffusion in the electrochemical mechanism, which are commonly described as Warburg behavior. On the other hand, from the high up to low frequency domains, all specimens have depicted a similar predominant capacitive behavior [47]. The largest phase angle suggests that Cu/20SiC has a higher barrier effect against the entry of

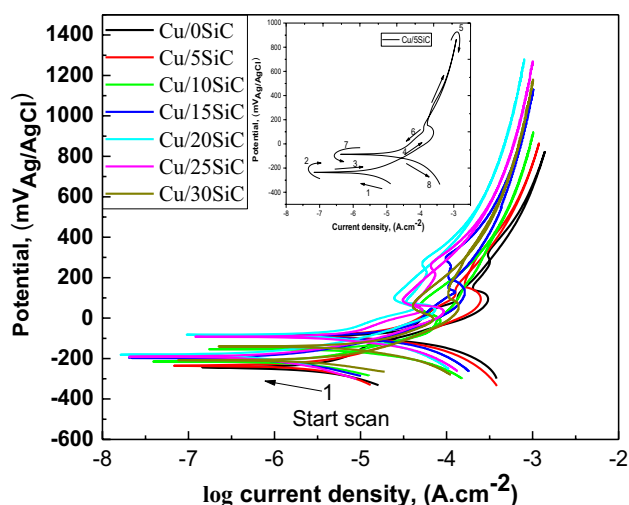


Fig. 12 Cyclic polarization curves of Cu matrix with different SiC contents in 3.5 wt% NaCl solution

corrosive ions. In order to provide “quantitative support” to the experimental EIS results, impedance parameters were obtained by the Echem Analyst™ software, adopting a well-known electrical equivalent circuit (EEC), which is shown in Fig. 10d [48–50]. Since an equivalent circuit is used in order to determine the simulated values and compare them with experimental data, a CNLS (complex non-linear least squares) simulation is used. The fitting quality was evaluated by Chi-squared (χ^2) values of about 10^{-4} , as shown in Table 2. This EEC is comprised of the Eq. (6) listed below:

$$Z_{tot} = R_u + \frac{1}{\frac{1}{R_p} + \frac{1}{Q_{dl}} + \frac{1}{W_d}} \quad (6)$$

where Z_{tot} , R_u , R_p , Q_{dl} , and W_d are the total impedance modulus, solution resistance, the resistance of charge transfer, the capacitance of double-layer, and Warburg diffusion impedance, respectively. In the EECs, the phase constant was used rather than pure capacitance owing to deviation from optimal conditions. The impedance Q_{dl} is computed using the next Eq. (7):

$$Q_{dl} = \frac{1}{Y_0} (j\omega)^{-n} \quad (7)$$

where Q_{dl} is the value of CPE, Y_0 signifies is the constant admittance of Q, j denotes the imaginary component, ω is the angular frequency, and n is the coefficient of dispersion associated with heterogeneous surfaces. According to electrochemical measurements, the polarization resistance (R_p) of Cu reinforced with ceramic phase rises with increasing SiC content up to 20%; Above this threshold, polarization resistance declines (Table 2). In contrast, the trend is

reversed for Cu/25SiC and Cu/30SiC because of the agglomeration and non-uniform distribution of the ceramic phase. The agglomerated ceramic reinforcing particles will produce concentration cells because of the potential differential between the reinforcing phase and reinforcement materials. Due to the large potential difference, galvanic cell formation takes place at agglomeration sites. Another justification for decrease anticorrosion resistance in Cu/25SiC composite is the existence of porosities or micro-cavities, which works as the nucleation sites and accelerate the corrosion process. These sites enable the corrosive anions to interact easily with the metal composite and produce corrosion products [48].

3.5 Potentiodynamic Polarization (PDP)

Figure 11 depicts the PDP plots of Cu composite reinforced by different vol% of SiC particles. The specimens were soaked in 3.5 wt% NaCl electrolyte. The plots consist of both cathodic and anodic graphs. The cathodic graphs are associated with the decrease of oxygen on the surface of the Cu composite, according to the next Eq. (8) [22]:



The findings indicated that the cathodic current significantly decreased to a lower value with an increase in vol% of SiC particles up to 20%. This suggests that Cu/20SiC inhibits the hydrogen reaction and improves its corrosion resistance compared with other specimens. On the other hand, the main anodic reaction of Cu in 3.5 wt% NaCl solution is illustrated in the following Eq. (9) [22]:

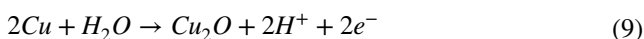


Table 3 summarizes the electrochemical characteristic derived from the Tafel plots, which included corrosion potential (E_{corr}), corrosion current density (i_{corr}), corrosion rate (mmy^{-1}), and anodic and cathodic slopes (β_a and β_c) [51]. The resistance to polarization (R_p) was assessed using the Stern–Geary equation Eq. (10) [26]:

$$R_p = \frac{\beta_a \times \beta_c}{2.303 \times i_{\text{corr}} \times (\beta_a + \beta_c)} \quad (10)$$

The components of the last Eq. (10) were described in detail in the previous paragraph [52]. According to Fig. 11 and Table 3, the i_{corr} lowers with increment SiC content up to 20 vol%. This behavior is attributable to many reasons as follows: (i) the uniform dispersion of SiC particles decline the effective net area exposed to the corrosive ions and act as a physical barrier owing to their extremely low chemical reactivity. Consequently,

the chemical activity of the composite is reduced, and the passivation of the matrix is enhanced. The behavior results in a reduction of the corrosion rate of the composite [53]. (ii) Schubert et al. [54] reported that instability of SiC at high temperature (the sintering process in our work) leads to migration of Si that diffuses into Cu matrix and forms Cu–Si solid solution. The latter has corrosion resistance better than pure Cu. (iii) the high purity of the SiC reinforcing particles increases the electrical resistivity of SiC. This minimizes the possibility of a cathodic reaction on the exterior of these particulates. (vi) the formation of interfacial corrosion products decouples the ceramic reinforcing from the composite alloy. Accordingly, no redox reaction between the composite and strengthened particles is anticipated, and the likelihood of the development of intermetallic phases is relatively low. These reasons diminish the composite's corrosion rate. On the other hand, Fig. 12 and Table 3 reveal also that when the vol% of SiC in the sintered specimen increases to 20 vol%, the E_{corr} moves to more noble/positive potential. The improvement in E_{corr} value indicates that the passivity of the alloy has been augmented owing to the creation of a thick and dense layer of patina on the surface. The slopes of the anodic and cathodic Tafel changed with increasing SiC particles. This suggests SiC ceramic phase significantly affects both anodic and cathodic responses [55, 56]. However, the findings illustrate that when SiC content increases more than 20 vol% in the matrix, the i_{corr} increases and E_{corr} shifts to lower values. This trend may be attributed to instability of SiC and migration of Si that leads to producing free C which with a considerable content may deteriorate the corrosion behavior where C acts as a cathodic phase [54]. Or due to the agglomeration of SiC which exerts defects in the patina structure.

3.6 Cyclic Polarization Technique (CPT)

The effect of SiC content on pitting potential and passive stability of Cu was investigated using CPT. Figure 12 illustrates the CPT graphs of the Cu/SiC composite in a 3.5 wt% NaCl solution. The plots reveal the cathodic current decrease with increment SiC percentage in MMCs. Furthermore, the anodic plots exhibit active, passive, trans-passive, and re-passive behavior. When the SiC content increases up to 20 vol%, the passivity zone increases. This behavior is caused by patina, which works as a passive layer to prevent further deterioration. Increasing SiC content over 20% in Cu MMCs reduces the passive range due to defects that exist in the patina structure. The patina layers that are deposited on the surface of the Cu/SiC specimens are formed according to Eqs. (11–13) [57]:

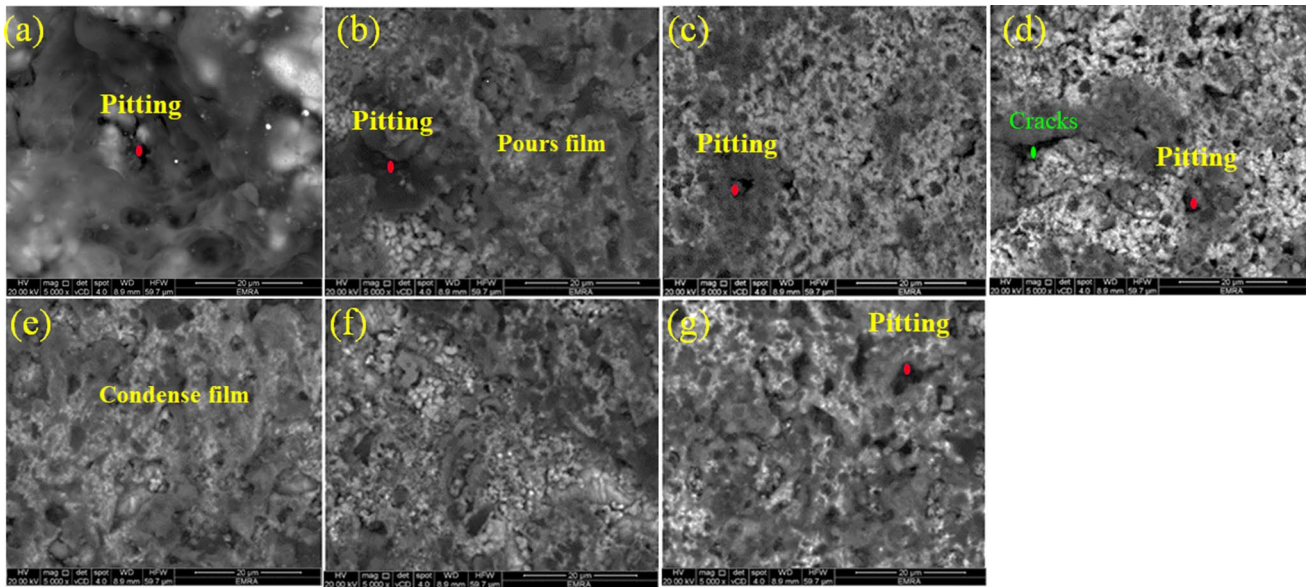


Fig. 13 Surface morphology of Cu/SiC composite with different SiC contents. (a 0 vol%, b 5 vol%, c 10 vol%, d 15 vol%, e 20 vol%, f 25 vol%, and g 30 vol% of SiC particulates)

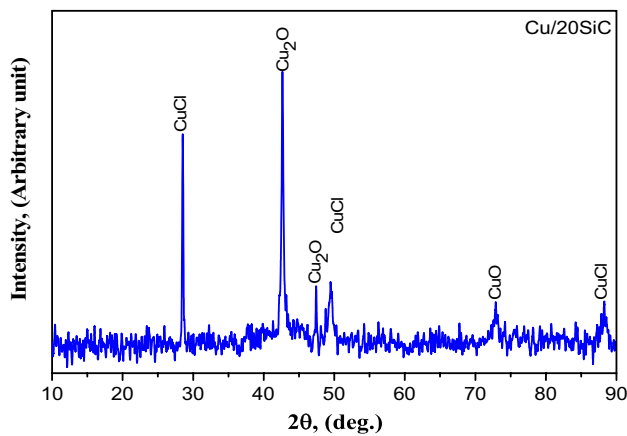
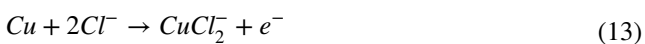


Fig. 14 X-ray diffraction of Cu composite reinforced with 20 vol% SiC particles



The existence of a high concentration of CuCl_2 at the surface causes hydrolysis of CuCl_2 and the creation of Cu_2O (Eq. 14) [57]:

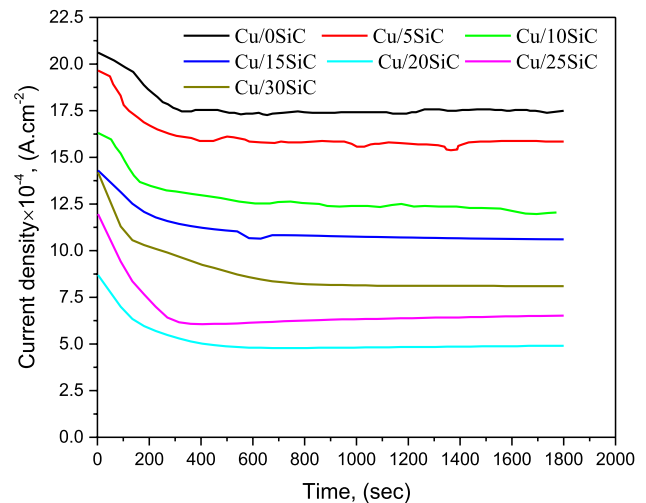
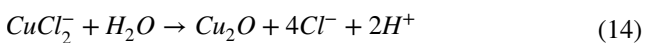


Fig. 15 Current–time curves of base matrix and its composite at 300 $\text{mV}_{\text{Ag/AgCl}}$

On the other hand, Fig. 12 demonstrates that the reverse anodic graphs of Cu/SiC composites are moved to higher currents. Consequently, pitting is anticipated for the examined specimens in 3.5 wt% NaCl electrolyte. The electrochemical characteristics derived from the cyclic polarization graphs in 3.5 wt% NaCl solution are presented in Table 4. According to the findings, as the SiC content increases, the passive current drops, and the pitting potential (E_{pit}) moves towards a more noble direction, signifying the formation of a more protective passive film. The behavior as mentioned

in the above sections is due to a uniform dispersion of SiC particles that declines the effective net area exposed to the corrosive ions and act as a physical barrier owing to their extremely low chemical reactivity. Accordingly, the chemical activity of the composite decreases and the passivation of the matrix is improved. However, the findings show that the passive zone is declined when the SiC content is increased more than 20 vol% because of instability of SiC with Cu at elevated temperature, producing free C which with a considerable content weaken the passive layer [53].

Figure 13a–g depicts surface morphologies of Cu MMCs reinforced by various vol% of SiC particles after cyclic polarization tests. It is obvious from Fig. 13a that the surface of the unreinforced Cu matrix deteriorated severely. Moreover, the patina created on the Cu matrix surface is subject to discontinuities in the surface. This is owing to the dissimilarity in the crystallographic structure of the surfaces. On the other hand, the Cu/xSiC composites exhibit pitting at different sites where the SiC particles agglomerate. The superior corrosion resistance of Cu/SiC composites comparing with pure Cu matrix may be ascribed to SiC particles being ceramics material and staying inert in a corrosive medium. The corroded surface (Fig. 13e) shows that the corrosion rate of the Cu/20SiC alloy composite is lower than that of the Cu matrix and the Cu/xSiC composites. The SEM images also show the creation of pits on the surface of the composites. However, the number of pits decreases with further SiC particulates. Additionally, it is appeared that increasing the amount of SiC particulates reduces the number of pits. This demeanor is attributable to the homogenous dispersion of SiC particulate within the Cu matrix, which hinders corrosive ions from reaching composite across patina. Also, the corroded morphologies of Cu/25SiC and Cu/30SiC composites show severe pitting and collapse of the patina layer formed in a few places due to the agglomeration of SiC reinforcing particulate within the Cu-matrix [26, 44]. Figure 14 represents the XRD spectra of Cu/20SiC composites after cyclic polarization examinations in 3.5 wt% NaCl electrolyte. The XRD diffractometer detects CuO, Cu₂O, and CuCl₂ diffraction peaks on the corroded surface of the Cu/20SiC composite. This result is consistent with Eqs. (11–14).

3.7 Potentiostatic-Time Measurements

Potentiostatic technique was conducted to investigate the electrochemical performance of the patina formed on Cu/SiC composites. Figure 15 presents the current density (A cm⁻²) of Cu and the composites reinforced with various SiC micro-sized as a function in immersion time. The

Cu/SiC specimens were immersed in a medium containing 3.5 wt% NaCl at an anodic potential of 0.3 V_{Ag/AgCl}. Firstly, the current densities for all specimens decrease by the creation of patina passive layers. Then, all composite specimens display a steady-state electrical current density due to the completion of the passive layer formation. According to the results, the current density of specimens reduces as the SiC content increases to 20% and then increases. The current density values settle at about (17.47, 15.90, 12, 10.6, 4.80, 8.11, and 6.48) × 10⁻⁴ A cm⁻² for the composite specimen synthesized with 5, 10, 15, 20, 25, and 30 vol% SiC, respectively. That is, reinforcing particles prevent Cl⁻ species from penetrating and inhibit charge transfer in corrosion reactions. The behavior is related to the homogeneous distribution of hard SiC reinforcing particles and good bonding with the Cu composite. Notably, the patina film generated on corrosion products not only prevents aggressive anions from penetrating but also hinders the charge transport of the redox reactions. After that, the passive current density increases with increment SiC content over 20% in copper composites owing to the cluster of SiC reinforcing particles and weak bonding between SiC and Cu matrix. The outcomes correspond to the polarization measurements in the earlier section [58–60].

4 Conclusions

In the present study, microstructure, corrosion, and electrochemical properties of Cu/SiC composites in 3.5 wt% NaCl solution were examined. The following conclusions can be drawn based on the experimental findings of this study:

- The sintered density of Cu composites decreased somewhat as the SiC particle content increased from 0 to 30 vol%. The measured densities ranged between 8.48 and 6.25 g/cm³ for Cu/0SiC and Cu/30SiC, respectively, depending on the SiC content.
- The hardness of the composite was improved significantly with increasing the amount of SiC reinforcement particles up to 20 vol% SiC. Incorporating further SiC particles subsequently the hardness was reduced.
- EIS, PDP and CPT findings suggested that the SiC acts as a more effective barrier against corrosion of Cu/SiC composite in 3.5 wt% NaCl solution.
- Incorporating 20 vol% SiC in Cu is seemed to be its optimum proportion for the fabrication of Cu/SiC composites. Incorporating further SiC particles declines their corrosion resistance.

- The passive zone of Cu/SiC increased with increasing SiC content up to 20 vol%. Above this value, it decreased but remained higher than its base matrix.

Author contributions MMS Formal analysis, Characterization, Investigation, Writing—review and editing. SMF Corrosion studies, Investigation, Writing an original draft—review and editing. MT Sample preparation, Investigation. IGE Formal analysis, Characterization, Investigation.

Funding Open access funding provided by The Science, Technology & Innovation Funding Authority (STDF) in cooperation with The Egyptian Knowledge Bank (EKB).

Declarations

Conflict of interest There is no conflict between authors and any person or authorities, and the authors own the research idea and its results. Therefore, we here confirm that: The article is original. The article has been written by the stated authors, who are all aware of its content and approve its submission. The article has yet to be published previously. The article is not under consideration for publication elsewhere. No conflict of interest exists.

Open Access This article is licensed under a Creative Commons Attribution 4.0 International License, which permits use, sharing, adaptation, distribution and reproduction in any medium or format, as long as you give appropriate credit to the original author(s) and the source, provide a link to the Creative Commons licence, and indicate if changes were made. The images or other third party material in this article are included in the article's Creative Commons licence, unless indicated otherwise in a credit line to the material. If material is not included in the article's Creative Commons licence and your intended use is not permitted by statutory regulation or exceeds the permitted use, you will need to obtain permission directly from the copyright holder. To view a copy of this licence, visit <http://creativecommons.org/licenses/by/4.0/>.

References

1. J. Zhang, L. He, Y. Zhou, Highly conductive and strengthened copper matrix composite reinforced by $Zr_2Al_3C_4$ particulates. *Scr. Mater.* **60**, 976–979 (2009). <https://doi.org/10.1016/j.scriptamat.2009.02.026>
2. K.M. Zohdy, M.M. Sadawy, M. Ghanem, Corrosion behavior of leaded-bronze alloys in sea water. *Mater. Chem. Phys.* **147**, 878–883 (2014). <https://doi.org/10.1016/j.matchemphys.2014.06.033>
3. G. Cui, Q. Bi, S. Zhu, J. Yang, W. Liu, Tribological behavior of Cu-6Sn-6Zn-3Pb under sea water, distilled water and dry-sliding conditions. *Tribol. Int.* **55**, 126–134 (2012). <https://doi.org/10.1016/j.triboint.2012.06.007>
4. K.K. Alaneme, B.U. Odoni, Mechanical properties, wear and corrosion behavior of copper matrix composites reinforced with steel machining chips. *Eng. Sci. Technol. Int. J.* **19**, 1593–1599 (2016). <https://doi.org/10.1016/j.jestch.2016.04.006>
5. G. Celebi Efe, M. Ipek, S. Zeytin, C. Bindal, An investigation of the effect of SiC particle size on Cu-SiC composites. *Compos. Part B Eng.* **43**, 1813–1822 (2012). <https://doi.org/10.1016/j.compositesb.2012.01.006>
6. V. Rajkovic, D. Bozic, M.T. Jovanovic, Effects of copper and Al_2O_3 particles on characteristics of Cu- Al_2O_3 composites. *Mater. Des.* **31**, 1962–1970 (2010). <https://doi.org/10.1016/j.matdes.2009.10.037>
7. B. Tian, P. Liu, K. Song, Y. Li, Y. Liu, F. Ren, J. Su, Microstructure and properties at elevated temperature of a nano- Al_2O_3 particles dispersion-strengthened copper base composite. *Mater. Sci. Eng. A* **435–436**, 705–710 (2006). <https://doi.org/10.1016/j.msea.2006.07.129>
8. S. Buytoz, F. Dagdelen, S. Islak, M. Kok, D. Kir, E. Ercan, Effect of the TiC content on microstructure and thermal properties of Cu-TiC composites prepared by powder metallurgy. *J. Therm. Anal. Calorim.* **117**, 1277–1283 (2014). <https://doi.org/10.1007/s10973-014-3900-6>
9. S. Wang, X. Pang, X. Guo, C. Cheng, Y. Liu, Y. Zhang, Mechanical and tribological properties of WC particles reinforced Cu-20Zn matrix composites. *Powder Technol.* **406**, 117571 (2022). <https://doi.org/10.1016/j.powtec.2022.117571>
10. K.M. Shu, G.C. Tu, Fabrication and characterization of Cu-SiCp composites for electrical discharge machining applications. *Mater. Manuf. Process.* **16**, 483–502 (2001). <https://doi.org/10.1081/AMP-100108522>
11. M.A. Metwally, M.M. Sadawy, M. Ghanem, I.G. El-Batanony, The role of nano-SiC on microstructure and tribological properties of SiC/Cu nano-composite. *J. Eng. Res. Rep.* **15**, 35–44 (2020). <https://doi.org/10.9734/jerr/2020/v15i417153>
12. A.K. Sharma, R. Bhandari, C. Pinca-Bretotean, Impact of silicon carbide reinforcement on characteristics of aluminium metal matrix composite. *J. Phys. Conf. Ser.* **1781**, 012031 (2021). <https://doi.org/10.1088/1742-6596/1781/1/012031>
13. R. Zare, H. Sharifi, M.R. Saeri, M. Tayebi, Investigating the effect of SiC particles on the physical and thermal properties of Al6061/SiCp composite. *J. Alloys Compd.* **801**, 520–528 (2019). <https://doi.org/10.1016/j.jallcom.2019.05.317>
14. P. Samal, H. Tarai, A. Meher, B. Surekha, P.R. Vundavilli, Effect of SiC and WC reinforcements on microstructural and mechanical characteristics of copper alloy-based metal matrix composites using stir casting route. *Appl. Sci.* **13**, 1754 (2023). <https://doi.org/10.3390/app13031754>
15. R.A. Youness, M.A. Taha, Review on using powder metallurgy method for production of metal-based nanocomposites. *Egypt. J. Chem.* **64**, 7215–7222 (2021). <https://doi.org/10.21608/EJCHEM.2021.79970.3934>
16. A.K. Sharma, R. Bhandari, C. Pinca-Bretotean, A systematic overview on fabrication aspects and methods of aluminum metal matrix composites. *Mater. Today Proc.* **45**, 4133–4138 (2020). <https://doi.org/10.1016/j.matpr.2020.11.899>
17. G.A. Bagheri, The effect of reinforcement percentages on properties of copper matrix composites reinforced with TiC particles. *J. Alloys Compd.* **676**, 120–126 (2016). <https://doi.org/10.1016/j.jallcom.2016.03.085>
18. C.P. Samal, J.S. Parihar, D. Chaira, The effect of milling and sintering techniques on mechanical properties of Cu-graphite metal matrix composite prepared by powder metallurgy route. *J. Alloys Compd.* **569**, 95–101 (2013). <https://doi.org/10.1016/j.jallcom.2013.03.122>
19. J. Wang, L.N. Guo, W.M. Lin, J. Chen, S. Zhang, S. Da Chen, T.T. Zhen, Y.Y. Zhang, The effects of graphene content on the corrosion resistance, and electrical, thermal and mechanical properties of graphene/copper composites. *Xinxing Tan Cailiao/New Carbon Mater.* **34**, 161–169 (2019). [https://doi.org/10.1016/S1872-5805\(19\)60009-0](https://doi.org/10.1016/S1872-5805(19)60009-0)
20. M.R. Akbarpour, H. Mousa Mirabad, S. Alipour, Microstructural and mechanical characteristics of hybrid SiC/Cu composites with nano- and micro-sized SiC particles. *Ceram. Int.* **45**,

- 3276–3283 (2019). <https://doi.org/10.1016/j.ceramint.2018.10.235>
21. H.B. Mayya, D. Pai, V.M. Kini, N.H. Padmaraj, Effect of marine environmental conditions on physical and mechanical properties of fiber-reinforced composites—A review. *J. Inst. Eng. Ser. C* **102**, 843–849 (2021). <https://doi.org/10.1007/s40032-021-00676-w>
 22. D. Saber, K.A. El-Aziz, B.F. Felemban, A.H. Alghtani, H.T. Ali, E.M. Ahmed, M. Megahed, Characterization and performance evaluation of Cu-based/TiO₂ nano composites. *Sci. Rep.* **12**, 6669 (2022). <https://doi.org/10.1038/s41598-022-10616-y>
 23. S. Banerjee, S. Poria, G. Sutradhar, P. Sahoo, Corrosion behavior of AZ31-WC nano-composites. *J. Magnes. Alloy.* **7**, 681–695 (2019). <https://doi.org/10.1016/j.jma.2019.07.004>
 24. H. Torabi, R. Arghavanian, Investigations on the corrosion resistance and microhardness of Cu–10Sn/SiC composite manufactured by powder metallurgy process. *J. Alloys Compd.* **806**, 99–105 (2019). <https://doi.org/10.1016/j.jallcom.2019.07.245>
 25. G. Celebi Efe, S. Zeytin, C. Bindal, The effect of SiC particle size on the properties of Cu-SiC composites. *Mater. Des.* **36**, 633–639 (2012). <https://doi.org/10.1016/j.matdes.2011.11.019>
 26. A. Jamwal, P. Prakash, D. Kumar, N. Singh, K.K. Sadasivuni, K. Harshit, S. Gupta, P. Gupta, Microstructure, wear and corrosion characteristics of Cu matrix reinforced SiC–graphite hybrid composites. *J. Compos. Mater.* **53**, 2545–2553 (2019). <https://doi.org/10.1177/0021998319832961>
 27. ASTM E3-95, Standard practice for preparation of metallographic specimens (ASTM International, West Conshohocken, 1995)
 28. M. Shabani, M.H. Paydar, R. Zamiri, M. Goodarzi, M.M. Moshksar, Microstructural and sliding wear behavior of SiC-particle reinforced copper matrix composites fabricated by sintering and sinter-forging processes. *J. Mater. Res. Technol.* **5**, 5–12 (2016). <https://doi.org/10.1016/j.jmrt.2015.03.002>
 29. ASTM G1-90, Standard practice for preparing, cleaning, and evaluation corrosion test specimens (ASTM International, West Conshohocken, 1999)
 30. ASTM G31-72, Standard practice for laboratory immersion corrosion testing of Metals (ASTM International, West Conshohocken, 2004)
 31. W.R. Osório, E.S. Freitas, A. Garcia, EIS and potentiodynamic polarization studies on immiscible monotectic Al-In alloys. *Electrochim. Acta* **102**, 436–445 (2013). <https://doi.org/10.1016/j.electacta.2013.04.047>
 32. W.R. Osório, L.C. Peixoto, D.J. Moutinho, L.G. Gomes, I.L. Ferreira, A. Garcia, Corrosion resistance of directionally solidified Al-6Cu-1Si and Al-8Cu-3Si alloys castings. *Mater. Des.* **32**, 3832–3837 (2011). <https://doi.org/10.1016/j.matdes.2011.03.013>
 33. X.L. Zhang, Z.H. Jiang, Z.P. Yao, Y. Song, Z.D. Wu, Effects of scan rate on the potentiodynamic polarization curve obtained to determine the Tafel slopes and corrosion current density. *Corros. Sci.* **51**, 581–587 (2009). <https://doi.org/10.1016/j.corsci.2008.12.005>
 34. E. McCafferty, Validation of corrosion rates measured by the Tafel extrapolation method. *Corros. Sci.* **47**, 3202–3215 (2005). <https://doi.org/10.1016/j.corsci.2005.05.046>
 35. G. Celebi Efe, T. Yener, I. Altinsoy, M. Ipek, S. Zeytin, C. Bindal, The effect of sintering temperature on some properties of Cu-SiC composite. *J. Alloys Compd.* **509**, 6036–6042 (2011). <https://doi.org/10.1016/j.jallcom.2011.02.170>
 36. A.S. Prosviryakov, SiC content effect on the properties of Cu–SiC composites produced by mechanical alloying. *J. Alloys Compd.* **632**, 707–710 (2015). <https://doi.org/10.1016/J.JALLCOM.2015.01.298>
 37. N. Somani, N.K. Gupta, Effect of TiC nanoparticles on microstructural and tribological properties of Cu-TiC nano-composites. *Proc. Inst. Mech. Eng. Part B J. Eng. Manuf.* **236**, 319–336 (2022). <https://doi.org/10.1177/09544054211029828>
 38. H.R. Akramifard, M. Shamanian, M. Sabbaghian, M. Esmailzadeh, Microstructure and mechanical properties of Cu/SiC metal matrix composite fabricated via friction stir processing. *Mater. Des.* **54**, 838–844 (2014). <https://doi.org/10.1016/j.matdes.2013.08.107>
 39. M. Chmielewski, K. Pietrzak, A. Strojny-Nędza, K. Kaszyca, R. Zybala, P. Bazarnik, M. Lewandowska, S. Nosewicz, Microstructure and thermal properties of Cu-SiC composite materials depending on the sintering technique. *Sci. Sinter.* **49**, 11–22 (2017). <https://doi.org/10.2298/SOS1701011C>
 40. M.R. Akbarpour, F. Gharibi Asl, H. Mousa Mirabad, H.S. Kim, Microstructural characterization and enhanced tensile and tribological properties of Cu–SiC nanocomposites developed by high-pressure torsion. *J. Mater. Res. Technol.* **20**, 4038–4051 (2022). <https://doi.org/10.1016/j.jmrt.2022.08.141>
 41. Z.G. Wang, C.P. Li, H.Y. Wang, J.N. Zhu, C. Wang, Q.C. Jiang, Wear and corrosion behavior of functionally graded nano-SiC/2014Al composites produced by powder metallurgy. *J. Mater. Eng. Perform.* **26**, 729–735 (2017). <https://doi.org/10.1007/s11665-016-2466-9>
 42. N. Somani, N. Sharma, A. Sharma, Y.K. Gautam, P. Khatri, J.A.A. Solomon, Fabrication of Cu-SiC composites using powder metallurgy technique. *Mater. Today Proc.* **5**, 28136–28141 (2018). <https://doi.org/10.1016/j.matpr.2018.10.055>
 43. M. Zakaulla, A.R.A. Khan, P.G. Mukunda, Effect of electroless copper coating on the corrosion behavior of aluminium based metal matrix composites reinforced with silicon carbide particles. *J. Miner. Mater. Charact. Eng.* **2**, 21–25 (2014). <https://doi.org/10.4236/jmmce.2014.21004>
 44. H.M. Zakaria, Microstructural and corrosion behavior of Al/SiC metal matrix composites. *Ain Shams Eng. J.* **5**, 831–838 (2014). <https://doi.org/10.1016/j.asej.2014.03.003>
 45. Y.M. Han, X.G. Chen, Electrochemical behavior of Al-B4C metal matrix composites in NaCl solution. *Materials (Basel)* **8**, 6455–6470 (2015). <https://doi.org/10.3390/ma8095314>
 46. S.M. Fayed, P. Gao, D. Chen, S. Li, Y. Zhou, H. Wang, M.M. Sadawy, Corrosion inhibition characteristics of multilayer Si-DLC, phosphating and anodizing coatings deposited on 2024 Al alloy: a comparative study. *Diam. Relat. Mater.* **117**, 108460 (2021). <https://doi.org/10.1016/j.diamond.2021.108460>
 47. T. Duarte, Y.A. Meyer, W.R. Osório, The holes of Zn phosphate and hot dip galvanizing on electrochemical behaviors of multi-coatings on steel substrates. *Metals (Basel)* **12**, 863 (2022). <https://doi.org/10.3390/met12050863>
 48. B. Hirschorn, M.E. Orazem, B. Tribollet, V. Vivier, I. Frateur, M. Musiani, Constant-phase-element behavior caused by resistivity distributions in films. *J. Electrochem. Soc.* **157**, C458 (2010). <https://doi.org/10.1149/1.3499565>
 49. Y.A. Meyer, I. Menezes, R.S. Bonatti, A.D. Bortolozzo, W.R. Osório, EIS investigation of the corrosion behavior of steel bars embedded into modified concretes with eggshell contents. *Metals (Basel)* **12**, 417 (2022). <https://doi.org/10.3390/met12030417>
 50. Y.A. Meyer, R.S. Bonatti, A.D. Bortolozzo, W.R. Osório, Electrochemical behavior and compressive strength of Al-Cu/xCu composites in NaCl solution. *J. Solid State Electrochem.* **25**, 1303–1317 (2021). <https://doi.org/10.1007/s10008-020-04890-x>
 51. Z. Hamidi, S.Y. Mosavian, N. Sabbaghi, M.A. Karimi Zarchi, M. Noroozifar, Cross-linked poly(*N*-alkyl-4-vinylpyridinium) iodides as new eco-friendly inhibitors for corrosion study of St-37 steel in

- 1 M H₂SO₄. Iran. Polym. J. **29**, 225–239 (2020). <https://doi.org/10.1007/s13726-020-00787-8>
52. T. Rabizadeh, S.K. Asl, Casein as a natural protein to inhibit the corrosion of mild steel in HCl solution. J. Mol. Liq. **276**, 694–704 (2019). <https://doi.org/10.1016/j.molliq.2018.11.162>
53. S. Banthia, S. Sengupta, S. Das, K. Das, Cu, Cu-SiC functionally graded coating for protection against corrosion and wear. Surf. Coat. Tech. **374**, 833–844 (2019). <https://doi.org/10.1016/j.surfcoat.2019.06.050>
54. T. Schubert, A. Brendel, K. Schmid, T. Koeck, W. Zieliński, T. Weißgärber, B. Kieback, Interfacial design of Cu/SiC composites prepared by powder metallurgy for heat sink applications. Compos. Part A Appl. Sci. Manuf. **38**, 2398–2403 (2007). <https://doi.org/10.1016/j.compositesa.2007.08.012>
55. M.A. Almomani, W.R. Tyfour, M.H. Nemrat, Effect of silicon carbide addition on the corrosion behavior of powder metallurgy Cu-30Zn brass in a 3.5 wt% NaCl solution. J. Alloys Compd. **679**, 104–114 (2016). <https://doi.org/10.1016/j.jallcom.2016.04.006>
56. S.M. Fayed, H. Wu, D. Chen, S. Li, Y. Zhou, H. Wang, M.M. Sadawy, Influence of positive pulse voltages on structure, mechanical, and corrosion inhibition characteristics of Si/DLC coatings. Surf. Coat. Tech. **445**, 128749 (2022). <https://doi.org/10.1016/j.surfcoat.2022.128749>
57. L.C. Tsao, C.W. Chen, Corrosion characterization of Cu-Sn intermetallics in 3.5 wt% NaCl solution. Corros. Sci. **63**, 393–398 (2012). <https://doi.org/10.1016/j.corsci.2012.06.015>
58. M.M. Sadawy, E.A. Eid, Preparation and electrochemical behavior of graphene-oxide/zinc-phosphate composite coatings on as-cast Al-Zn (5.0 wt%)-Mg (2.5 wt%) alloy. Synth. Met. **259**, 116236 (2020). <https://doi.org/10.1016/j.synthmet.2019.116236>
59. S.M. Fayed, D. Chen, S. Li, Y. Zhou, H. Wang, M.M. Sadawy, Corrosion behavior and passive stability of multilayer DLC-Si coatings. Surf. Coat. Tech. **431**, 128001 (2022). <https://doi.org/10.1016/j.surfcoat.2021.128001>
60. M.E.-S. Sherif, Inhibition of copper corrosion reactions in neutral and acidic chloride solutions by 5-ethyl-1,3,4-thiadiazol-2-amine as a corrosion inhibitor. Int. J. Electrochem. Sci. **7**, 2832–2845 (2012). [https://doi.org/10.1016/S1452-3981\(23\)13918-6](https://doi.org/10.1016/S1452-3981(23)13918-6)

Publisher's Note Springer Nature remains neutral with regard to jurisdictional claims in published maps and institutional affiliations.